ACS OMEGA

http://pubs.acs.org/journal/acsodf

Article

Conformational Heterogeneity and Self-Assembly of α,β,γ-Hybrid Peptides Containing Fenamic Acid: Multistimuli-Responsive Phase-Selective Gelation

Srayoshi Roy Chowdhury, Sujay Kumar Nandi, Debasish Podder, and Debasish Haldar*

Cite This: *ACS Omega* 2020, 5, 2287−2294

Read Online

ACCESS | Metrics & More | Article Recommendations | Supporting Information

ABSTRACT: The effect of fenamic acid−α-aminoisobutyric acid corner motif in α,β,γ-hybrid peptides has been reported. From X-ray single-crystal diffraction studies, it is observed that Phe-containing peptide **1** has an "S"-shaped conformation that is stabilized by two consecutive intramolecular N−H···N hydrogen bonds. However, the tyrosine analogue peptide **2** has an "S"-shaped conformation, which is stabilized by consecutive intramolecular six-member N−H···N and seven-member N−H···O hydrogen bonds. The asymmetric unit of peptide **3** containing *m*-aminobenzoic acid has two molecules which are stabilized by multiple intermolecular hydrogen-bonding interactions. There are also π−π stacking interactions between the aromatic rings of fenamic acid. The peptides **1** and **2** have a polydisperse microsphere morphology, but peptide **3** has an entangled fiber-like morphology. Peptides **1**−**3** do not form organogels. However, in the presence of water, the peptide **3** forms a phase-selective instant gel in xylene. The gel exhibits high stability and thermal reversibility. The phase-selective gel of peptide **3** is highly responsive to H_2SO_4.

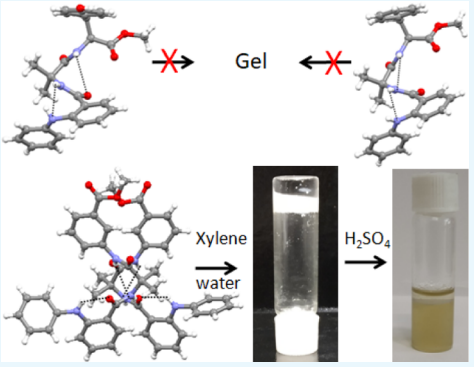

INTRODUCTION

Molecular conformations, the three-dimensional structures of molecules, are highly important to study the recognition and assembly process and have wide applications in medicine and materials science.[1] Among the molecular building blocks, the conformational analysis of peptides is highly challenging.[2] There are many factors that contribute to the molecular conformation of peptides. There are a large number of degrees of freedom for α-peptides. Also, the transannular interactions like hydrogen bonds, π−π stacking interactions, ionic interactions, and hydrophobic interactions play important roles.[3] Moreover, the range of steric interactions, steric hindrance, and geometrical rigidity is also crucial.[4,5] In this regard, the incorporation of noncoded β, γ, δ, or ε amino acids is very common for the design of hybrid peptides.[6−8] There are many examples that show how relatively small modifications have huge impact on conformational preferences.[9−12] Recently, Gopi and co-workers have discussed about the conformational analysis of peptides containing unsaturated aliphatic amino acids.[13] Previously, we have also reported the conformational studies and structural versatilities of small peptides.[14−18]

Phase-selective gelation has the potential to solve environmental issues like oil spill recovery from aquatic bodies and water purification by removing the pollutants.[19] The phase-selective organogelator has the potential to form a gel in one solvent, preferentially from the immiscible solvent mixture.[20] In 2001, an amino acid amphiphile-based phase-selective gel was reported by Bhattacharya and Krishnan-Ghosh.[21] Since then, various phase-selective organogelators have been developed.[22−26] However, most of them have some limitations for real-time use.

Previously, we have reported the phase-selective gelation and fabrication of nanoporous materials from a hydrophobic peptide.[27] Herein, a series of tripeptides containing fenamic acid and α-aminoisobutyric acid (Aib) have been synthesized. Although fenamic acid has been widely studied in biology,[28,29] very little is known about the conformational properties. Aib is conformationally rigid and helicogenic in nature. Fenamic acid is also geometrically not very flexible. Hence, the incorporation of Aib and fenamic acid in a peptide backbone will be done for the molecular structure as well as for the direction of molecular orientation and self-assembly (Figure 1).

RESULTS AND DISCUSSION

The α,β-hybrid peptides **1**−**3** were synthesized by the solution-phase peptide synthesis process using N,N'-dicyclohexylcarbo-

Received: October 22, 2019
Accepted: January 17, 2020
Published: January 30, 2020

https://dx.doi.org/10.1021/acsomega.9b03532
ACS Omega 2020, 5, 2287−2294

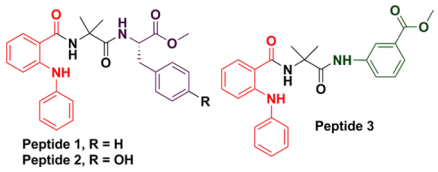

Figure 1. Chemical structures of α,β-hybrid peptides **1**−**3** (fenamic acid in red; Aib in black; Phe (for peptide **1**) and Tyr (for peptide **2**) in violet; and Maba in green).

diimide (DCC) as a coupling reagent (Figure S1). Fenamic acid was incorporated in the N-terminus, without any protecting group. Peptide **1** contains L-phenylalanine (Phe), and peptide **2** is a L-Tyrosine (Tyr) analogue of peptide **1**. However, peptide **3** contains an *m*-aminobenzoic acid (Maba) at the C-terminus. Helicogenic α-amino isobutyric acid was incorporated to increase the conformational rigidity and crystallinity. All the synthesized peptides and intermediates were purified by column chromatography and characterized by Fourier transform infrared spectroscopy (FT-IR), ^{1}H nuclear magnetic resonance (NMR), ^{13}C NMR spectroscopy, and mass spectrometry.

We have used different spectroscopic techniques to study the self-assembly propensities of the α,β-hybrid peptides **1**−**3** in solution. The solution-state UV/vis experiments for peptide **2** show no change of spectral positions for π-to-π^* transition (288 and 338 nm), but absorbance increases with an increasing peptide concentration in methanol solution (Figure S3). The peptides **1** and **3** show absorption bands at 288 and 346 nm and 288 and 342 nm, respectively. Here also, the intensity of absorption increases with the corresponding increase in peptide concentration in methanol solution (Figures S2 and S4), without any band shift. On excitation at 338 nm, peptide **2** exhibits emission peaks at 410 and 427 nm (Figure S3). From Figure S3, it is observed that the intensity of emission increases with the increasing peptide concentration in methanol solution. Peptides **1** and **3** also show similar emission properties (Figures S2 and S4).

The morphology of the α,β-hybrid peptides was examined by polarized optical microscopy (POM). The POM images show that peptides **1** and **2** have microsphere morphology, but peptide **3** depicts branched fibril-like morphology (Figure S5). Further, field emission scanning electron microscopy (FE-SEM) was performed. For FE-SEM measurements, dilute solutions (0.5 mM) of the corresponding peptides **1**−**3** were drop-casted on clean microscopic glass slides and carefully dried under a vacuum for 48 h. Figure 2 exhibits the FE-SEM images of the peptides **1**−**3**. From Figure 2a,b, it is observed that the peptides **1** and **2** show polydisperse microsphere morphology. The average diameter of the microspheres is ca. 500 nm for peptide **1** and ca. 200 nm for peptide **2**. From Figure 2c,d, it is observed that peptide **3** exhibits an entangled fibril-like morphology. The diameter of the fibrils is ca. 1 μm and the length is of several micrometers.

To know the information about the backbone structure and the self-assembly patterns of peptides, FT-IR spectroscopy was performed. The α,β-hybrid peptide **1** exhibits N−H stretching vibrations at 3305 cm^{-1} and amide I and amide II peaks at 1664 and 1602 cm^{-1}.[30] However the α,β-hybrid peptide **2** shows N−H stretching vibration at 3308 cm^{-1} and amide I and amide II peaks at 1670 and 1601 cm^{-1} (Figure 3).[21] The α,β,γ-hybrid peptide **3** exhibits N−H stretching vibration at 3315 cm^{-1} and amide I and amide II peaks at 1669 and 1590 cm^{-1}.

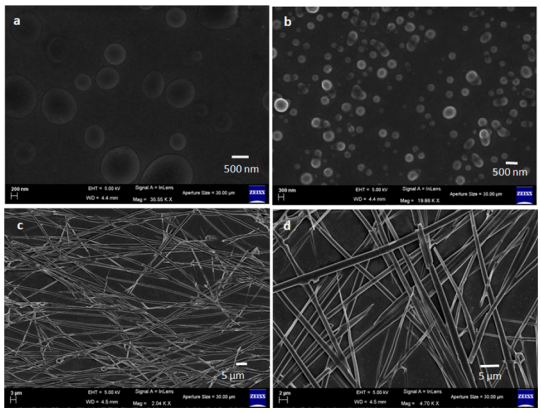

Figure 2. FE-SEM images of (a) peptide **1** showing polydisperse microsphere morphology, (b) peptide **2** showing polydisperse microsphere morphology, and (c,d) peptide **3** showing entangled fiber-like morphology.

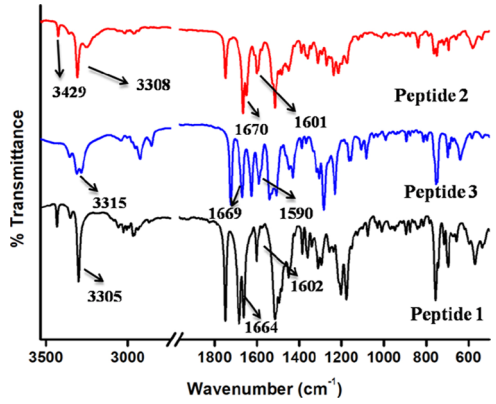

Figure 3. FT-IR spectra of peptides **1**−**3**.

For peptides **1** and **2**, the peak at 3429 cm^{-1} indicates that all N−H's are not hydrogen-bonded.

Single-crystal X-ray diffraction analysis was performed to explore the backbone conformation and self-assembly pattern of the fenamic acid-containing α,β-hybrid peptides **1**−**3**. Colorless monoclinic crystals of peptide **1** suitable for X-ray crystallography were obtained from methanol−water solution by slow evaporation. There is one molecule of peptide **1** in the asymmetric unit (Figure 4a). The peptide **1** adopts an "S"-shaped conformation and is stabilized by two consecutive intramolecular N−H···N hydrogen bonds (Figure 4a). A strong $\pi-\pi$ stacking interaction (shortest C−C distance of 3.20 Å) also stabilized the "S"-shaped conformation. The ϕ and ψ values of the Aib residues are in the right-handed helical region of the Ramachandran diagram. In higher-order assembly, the peptide **1** molecules self-assemble through multiple N−H···O intermolecular hydrogen bonds to form a parallel sheet-like structure (Figure 4b). Table 1 exhibits the crucial backbone torsion angles of peptide **1**. Table 2 shows the hydrogen-bonding parameters of peptide **1**.

Colorless monoclinic crystals of peptide **2** were obtained from the hexane−dichloromethane (DCM) solution by slow evaporation. From X-ray crystallography, it is observed that the α,β-hybrid peptide **2** adopts an "S"-shaped conformation in solid state. There is one molecule of peptide **2** in the asymmetric unit (Figure 5a). The ϕ and ψ values of the Aib residues are in the right-handed helical region of the

https://dx.doi.org/10.1021/acsomega.9b03532
ACS Omega 2020, 5, 2287−2294

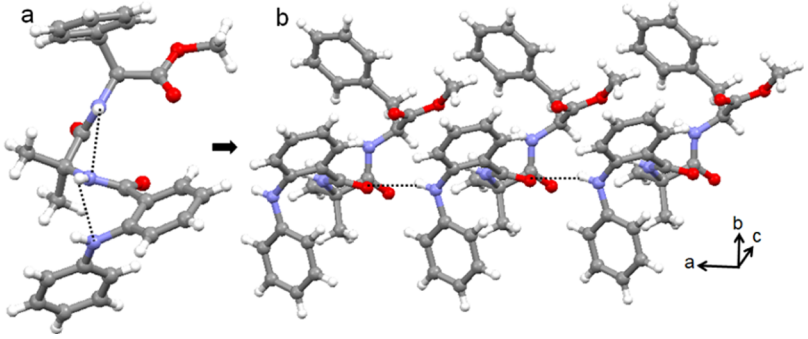

Figure 4. (a) Solid-state conformation of α,β-hybrid peptide **1** and (b) parallel sheet-like arrangement of peptide **1** molecules along the crystallographic *a* direction. Hydrogen bonds are shown as dotted lines.

Table 1. Important Backbone Torsion Angles (deg) for Peptides 1−3

	ϕ_1/deg	ψ_1/deg	ϕ_2/deg	ψ_2/deg	ϕ_3/deg	ψ_3/deg
1	61.37	42.67	−56.36	−38.97	−116.81	167.23
2	57.42	43.65	−58.44	−33.84	−123.77	169.87
3A	177.41	146.74	48.20	50.34	−37.52	10.79
3B	−177.95	−145.99	−50.74	−49.52	40.51	1.92

Table 2. Hydrogen-Bonding Parameters for Peptides 1−3

	D−H···A	D···H(Å)	H···A (Å)	D···A (Å)	D−H···A (deg)
1	N2−H2···N1	0.8600	2.5100	2.895(5)	108.00
	N3−H3···N2	0.8600	2.4500	2.761(5)	102.00
	N1−H1···O1	0.8600	2.2200	2.918(5)	139.00[a]
2	N6−H6···N7	0.8600	2.5600	2.919(4)	106.00
	N8−H8···N6	0.8600	2.3800	2.718(4)	104.00
	O4−H4···O2	0.8200	1.9000	2.715(4)	176.00[b]
3	N6−H6···O2	0.8600	2.1600	2.969(7)	156.00
	N6−H6···N5	0.8600	2.5300	2.833(8)	101.00
	N5−H5···O1	0.8600	1.9800	2.823(6)	164.00
	N3−H3···N2	0.8600	2.5500	2.840(8)	101.00
	N1−H1···O1	0.8600	2.0900	2.706(7)	128.00
	N4−H4···O5	0.8600	2.0800	2.724(8)	131.00
	N2−H2···O5	0.8600	2.0800	2.922(6)	165.00[c]
	N3−H3···O6	0.8600	2.0800	2.897(6)	158.00[c]

Symmetry equivalent: $a = 1 + x, y, z$; $b = x, y, 1 + z$; $c = x, -1 + y, z$.

Ramachandran plot. The important backbone torsion angles of peptide **2** are listed in Table 1. The "S"-shaped conformation of peptide **2** is stabilized by consecutive intramolecular N−H···N and N−H···O hydrogen bonds (Figure 5a). A strong $\pi-\pi$ stacking interaction (shortest C−C distance of 3.10 Å) also stabilized the "S"-shaped conformation. In higher-order packing, the peptide **2** molecules self-assemble to form a parallel sheet-like structure (Figure 5b) through intermolecular O−H···O hydrogen-bonding interactions. The hydrogen-bonding parameters of peptide **2** are listed in Table 2.

The colorless monoclinic crystals of peptide **3** were obtained from acetonitrile solution by slow evaporation. There are two molecules of peptide **3** in the asymmetric unit (Figure 6). The

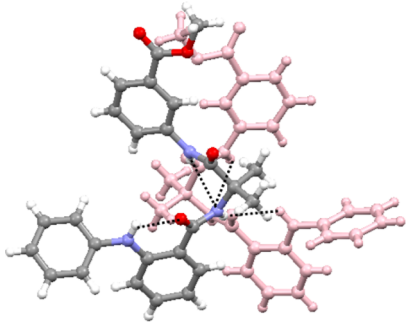

Figure 6. Solid-state conformations of the α,β,γ-hybrid peptide **3** molecules in the asymmetric unit. To visualize and understand, the different peptide **3** units appeared with different colors. Hydrogen bonds are shown as dotted lines.

ϕ and ψ values of the Aib residue of molecule A are in the right-handed helical region, whereas the ϕ and ψ values of the Aib residue of molecule B are in the left-handed helical region of the Ramachandran diagram. Table 1 exhibits the crucial backbone torsion angles for the molecules A and B of peptide **3**. The "S"-shaped conformation of peptide **3** molecules is

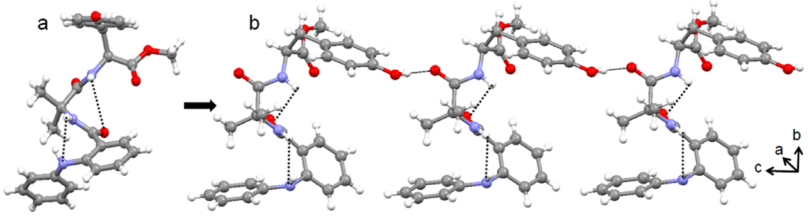

Figure 5. (a) Solid-state conformation of α,β-hybrid peptide **2** and (b) parallel sheet-like arrangement of peptide **2** molecules along the crystallographic *c* direction. Hydrogen bonds are marked as dotted lines.

https://dx.doi.org/10.1021/acsomega.9b03532
ACS Omega 2020, 5, 2287−2294

stabilized by consecutive intramolecular six-member N−H···O and five-member N−H···N hydrogen bonds (Figure 6). Strong $\pi-\pi$ stacking interactions (shortest C−C distances are 3.19 Å for molecule A and 2.90 Å for molecule B) also stabilized the "S"-shaped conformations. Moreover, the duplex is also stabilized by intermolecular N−H···O hydrogen bonds between fenamic acid C═O and Aib NH and Aib C═O and Maba NH (Figure 6). Table 2 exhibits the hydrogen-bonding parameters of peptide **3**.

In higher-order packing, the peptide **3** duplexes further self-assembled through multiple intermolecular $\pi-\pi$ stacking interactions to form a two-dimensional layer structure (Figure 7) along crystallographic *a* and *c* directions.

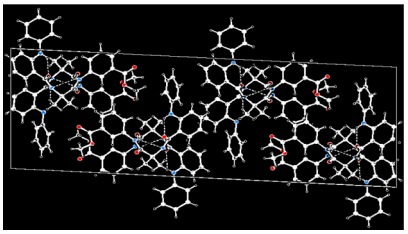

Figure 7. Two-dimensional layer structure of peptide **3** along the crystallographic *a* and *c* directions.

The α,β-hybrid peptides **1**−**3** failed to form an organogel. The α,β-hybrid peptides **1**−**3** form a clear solution on heating in aromatic solvents such as toluene, benzene, xylene, chlorobenzene, 1,2-dichlorobenzene, and nitrobenzene and precipitated out of the solution on cooling. Even the α,β-hybrid peptides **1**−**3** do not form a gel in an organic solvent at a very high concentration on sonication. However, peptide **3** was found to from a gel in an organic solvent and water mixture. In a usual procedure, a mixture of 1 mL of xylene and 1 mL of water was shaken in a test tube, and 25 mg of peptide **3** was added. The test tube was heated to dissolve the peptide **3** in the organic phase (xylene), followed by vigorous shaking to make a homogeneous dispersion. Surprisingly, on cooling at room temperature, the organic phase gelated, entrapping the water phase inside the test tube (Figure 8). However, the α,β-hybrid peptides **1** and **2** only provide viscous solutions even at very high concentrations.

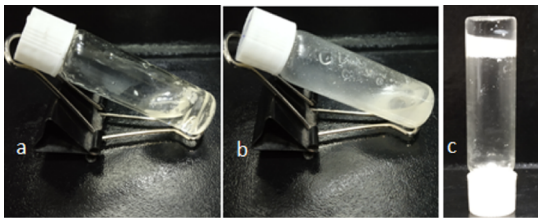

Figure 8. α,β,γ-Hybrid peptides (a) **1** and (b) **2** show viscous solutions in xylene/water mixture. (c) Inverted vial confirms the phase-selective gelation of α,β,γ-hybrid peptide **3** from the xylene/water mixture.

The phase-selective gelation of peptide **3** was confirmed by the inverted test tube method. The phase-selective gel is white, opaque, and stable for weeks. The phase-selective gel is thermoreversible in nature. The gel−sol transition temperature (T_{gel}) of the peptide **3** in xylene increases with increasing gelator concentration (Figure 9), a characteristic feature of low-molecular-weight gels.[31]

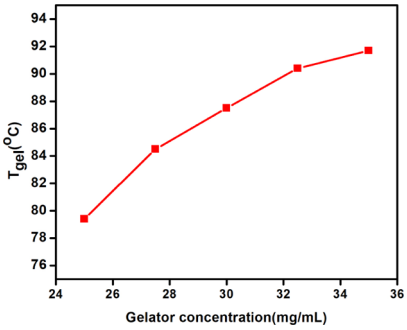

Figure 9. Change of gel−sol transition temperature (T_{gel}) of the peptide **3** in xylene with increasing gelator concentration.

The morphology of the xerogel was examined by transmission electron microscopy (TEM) measurements. For TEM experiments, a slice of the phase-selective gel was placed on a copper grid and finally dried under a vacuum for 2 days. Figure 10 depicts the TEM images of the peptide **3** xerogel. From

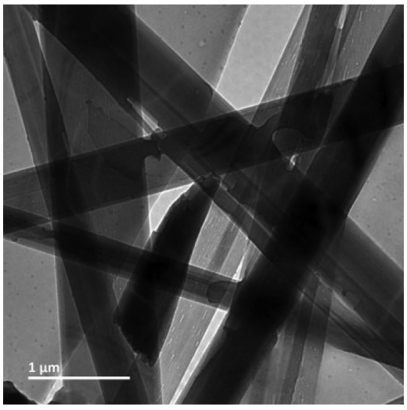

Figure 10. TEM images of the xerogel of α,β,γ-hybrid peptide **3** from xylene/water mixture showing a ribbon-like entangled network.

Figure 10, it is observed that the peptide **3** xerogel from xylene exhibits a ribbon-like morphology. The diameter of the ribbon is ca. 500 nm, and the length is of several micrometers. FT-IR spectroscopy shows that the backbone structure and the self-assembly pattern of the α,β,γ-hybrid peptide **3** in xerogel is almost the same as that in crystal (Figure S6). Hence, on phase-selective gelation, there is no change of backbone structure.

The phase-selective gel of α,β,γ-hybrid peptide **3** is responsive to H_2SO_4. On dropwise addition of H_2SO_4, the gel melts and finally forms a clear solution in the organic layer. However, the aqueous layer turns yellowish in color (Figure 11). This is due to the formation of a sulfate salt of diphenyl amine which is highly soluble in water (Figure S7). The response of the gel to HCl is comparatively slow. However, acetic acid has no effect on the gel. This H_2SO_4-responsive melting of gel is interesting for oil spill recovery from water. All previous reports used tedious methods like distillation for oil spill recovery.[3233]

https://dx.doi.org/10.1021/acsomega.9b03532
ACS Omega 2020, 5, 2287−2294

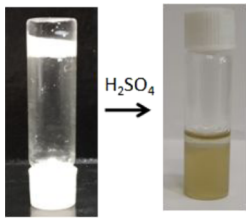

Figure 11. H_2SO_4-responsive gel-to-sol transformation.

CONCLUSIONS

In conclusion, we have discussed the effect of geometrically rigid fenamic acid−Aib corner motif in α,β-hybrid peptides. Though fenamic acid has been widely investigated in biology, very little is known about its conformational properties. From X-ray single-crystal diffraction studies, it is observed that the α,β-hybrid peptide **1** has an "S"-shaped conformation that is stabilized by two consecutive intramolecular N−H···N hydrogen bonds. However, the tyrosine analogue α,β-hybrid peptide **2** has an "S"-shaped conformation, which is stabilized by consecutive intramolecular six-member N−H···N and seven-member N−H···O hydrogen bonds. The asymmetric unit of α,β,γ-hybrid peptide **3** containing Maba has two molecules, which are stabilized by intermolecular hydrogen-bonding interactions and $\pi-\pi$ stacking of the fenamic acid aromatic rings. The peptides **1** and **2** have polydisperse microsphere morphology, but peptide **3** has entangled fiber-like morphology. Peptides **1**−**3** do not form an organogel by normal heating−cooling cycle or sonication. However, in the presence of water, the peptide **3** forms a phase-selective instant gel in xylene. The gel exhibits high stability and thermal reversibility and is highly sensitive to H_2SO_4. This is used in oil spill recovery. This result is particularly important for the future design of peptides with meaningful structure/activity relationships.

EXPERIMENTAL SECTION

General. All reagents were collected from SRL.

Peptide Synthesis. All the peptides were synthesized by solution-phase methodology. The C-terminus of peptides was protected by the formation of methyl ester. DCC was used as the coupling agent. The products were purified using column chromatography, with silica gel (mesh size 100−200) acting as a stationary phase and *n*-hexane−ethyl acetate solution as an eluent. ^{1}H NMR (400 and 500 MHz) and ^{13}C NMR (100 and 125 MHz) spectroscopy, mass spectrometry, and FT-IR spectroscopy analyses were used to characterize the reaction intermediates and final peptides. Further, the peptides **1**−**3** were characterized by X-ray crystallography.

Fenamic Acid−Aib OMe (NPA-Aib-OMe). A 2.7 g (13 mmol) of NPA-OH was dissolved in 25 mL of dry DCM in an ice−water bath. A 3.3 g (16 mmol) of DCC was added to the reaction mixture. H-Aib-OMe was extracted from 2.6 g (17 mmol) of the corresponding methyl ester hydrochloride by neutralization and subsequent extraction with ethyl acetate; ethyl acetate was evaporated, and then it was dissolved in dry DCM and added to the reaction mixture immediately after the addition of DCC. The reaction mixture was placed to come to room temperature and stirred for 48 h. After monitoring the reaction by thin-layer chromatography (TLC), DCM was evaporated, and the residue was dissolved in ethyl acetate (60 mL). Then, dicyclohexyl urea (DCU) was filtered off; 2 M HCl (3 × 50 mL), brine (2 × 50 mL), 1 M sodium carbonate (3 × 50 mL), and brine (2 × 50 mL) were used to wash the organic layer, and the organic layer was dried over anhydrous sodium sulfate and evaporated in a vacuum to obtain the compound NPA-Aib-OMe as a white solid. Silica gel (100−200 mesh) and hexane-ethyl acetate (19:1) as an eluent were used for the purification of the compound. Yield: 2.84 g (9.1 mmol, 70%). ^{1}H NMR (400 MHz, $CDCl_3$, δ ppm): 1.56 [s, 6H, Aib-C$^\beta$H], 3.68 [s, 3H, −OCH_3], 6.68 [s, 1H, Aib-NH], 6.71 [m, 1H, aromatic proton], 6.93 [m, 1H, aromatic proton], 7.12 [m, 2H, aromatic proton], 7.22−7.3 [m, 4H, aromatic proton], 7.38 [m, 1H, aromatic proton], 9.12 [s, 1H, NPA-NH]. ^{13}C NMR (100 MHz, $CDCl_3$, δ ppm): 25.32, 53.14, 57.09, 115.82, 118.27, 118.48, 121.38, 122.91, 128.27, 129.67, 132.73, 141.91, 146.03, 169.42, 175.58. Mass spectral data TOF-MS *m*/*z*: $[M + Na]^+$, 335.018.

Fenamic Acid−Aib OH (NPA-Aib-OH). A 1.6 g (5 mmol) of the NPA-Aib-OMe compound was dissolved in 25 mL of MeOH and 12.5 mL NaOH (2M) was added in the solution. Then, the reaction mixture was stirred, and TLC was used to monitor the progress of saponification. After completion of the reaction, methanol was evaporated under a vacuum; the residue was dissolved in 50 mL of water, and diethyl ether (2 × 50 mL) was used to wash the aqueous layer. Then, the pH of the aqueous layer was adjusted by using 1 M HCl, and the compound was extracted with ethyl acetate (3 × 50 mL). The extracts were dried over anhydrous sodium sulfate and evaporated under a vacuum to obtain the compound as a white solid. Yield: 1.3 g (4.6 mmol, 92%). ^{1}H NMR (500 MHz, DMSO-d_6, δ ppm): 1.44 [s, 6H, Aib-C$^\beta$H], 6.83 [m, 1H, aromatic proton], 6.96 [m, 1H, aromatic proton], 7.12 [m, 2H, aromatic proton], 7.28−7.31 [m, 4H, aromatic proton], 7.67 [m, 2H, aromatic proton], 8.56 [s, 1H, Aib-NH], 9.37 [s, 1H, NPA-NH], 12.24 [b, 1H, acid OH]. ^{13}C NMR (125 MHz, DMSO-d_6, δ ppm): 24.91, 55.47, 114.92, 118.1, 119.09, 119.38, 121.77, 129.4, 131.88, 141.53, 144.07, 168.46, 175.53. Mass spectral data TOF-MS *m*/*z*: $[M + Na]^+$, 321.0616.

*Fenamic Acid−Aib-Phe-OMe (Peptide **1**).* NPA-Aib-OH (500 mg, 1.68 mmol) was dissolved in 25 mL of dry DCM in an ice−water bath, and 0.7 g (3.35 mmol) of DCC and 0.45 gm (3.35 mmol) of HOBt were added in the reaction mixture. H-Phe-OMe was extracted from 0.7 g (3.35 mmol) of the corresponding methyl ester hydrochloride by neutralization and subsequent extraction with ethyl acetate, and ethyl acetate was evaporated; then, it was dissolved to dry DCM and added to the reaction mixture immediately after the addition of DCC and HOBt. The reaction mixture was allowed to come to room temperature and stirred for 48 h. Then, DCM was evaporated, the residue was dissolved in ethyl acetate (60 mL), and DCU was filtered off. A 2 M HCl (3 × 50 mL), 1 M sodium carbonate (3 × 50 mL), and brine (2 × 50 mL) were used to wash the organic layer, and the organic layer was dried over anhydrous sodium sulfate and evaporated in a vacuum to obtain peptide **1** as a solid. Silica gel (100−200 mesh) and hexane−ethyl acetate (4:1) as an eluent were used for the purification of the compound. Yield: 0.55 g (1.2 mmol, 70%). ^{1}H NMR (400 MHz, $CDCl_3$, δ ppm): 1.57 (s, 3H, Aib C$^\beta$H), 1.59 (s, 3H, Aib C$^\beta$H), 3.09 (m, 2H, Phe C$^\beta$H), 3.63 (s, 3H, Phe OMe), 4.88 (q, 1H, Phe C$^\alpha$H), 6.73 (m, 2H, aromatic proton), 6.83 (s, 1H, aromatic proton), 6.97 (m, 1H, Phe-NH), 7.06 (m, 2H, aromatic proton), 7.08−7.12 (m, 5H, aromatic proton), 7.16−7.3 (m, 4H, aromatic proton and Aib-NH), 7.4 (m, 1H, aromatic proton), 9.19 (b, 1H, NPA-NH),

https://dx.doi.org/10.1021/acsomega.9b03532
ACS Omega 2020, 5, 2287−2294

^{13}C NMR (100 MHz, $CDCl_3$, δ ppm): 25, 25.48, 37.94, 52.43, 53.29, 57.51, 115.79, 118.17, 118.27, 121.01, 122.65, 127.22, 128.12, 128.64, 129.40, 132.51, 135.86, 141.63, 145.72, 169.28, 172.01, 174.11. Mass spectral data TOF-MS m/z: $[M + Na]^+$, 482.1811.

*(d) Fenamic Acid−Aib-Tyr-OMe (Peptide **2**).* A 500 mg (1.68 mmol) of NPA-Aib-OH was dissolved in 25 mL of dry DCM in an ice−water bath. A 0.7 g (3.35 mmol) of DCC and 0.45 g (3.35 mmol) of HOBt were added in the reaction mixture. H-Tyr-OMe was extracted from 0.78 g (3.35 mmol) of the corresponding methyl ester hydrochloride by neutralization and subsequent extraction with ethyl acetate, and ethyl acetate was evaporated; then, it was dissolved to dry DCM and added to the reaction mixture immediately after the addition of DCC and HOBt. After coming to the room temperature, the reaction mixture was stirred for 48 h. Then, DCM was evaporated, the residue was dissolved in ethyl acetate (60 mL), and DCU was filtered off. A 2M HCl (3 × 50 mL), 1 M sodium carbonate (3 × 50 mL), and brine (2 × 50 mL) were used to wash the organic layer, and the organic layer was dried over anhydrous sodium sulfate and evaporated in a vacuum to obtain peptide **2** as a solid. Silica gel (100−200 mesh) and hexane−ethyl acetate (4:1) as an eluent were used for the purification of the compound. Yield: 0.52 g (1.1 mmol. 65%).^{1}H NMR (400 MHz, DMSO-d_6, δ ppm): 1.36 (s, 6H, Aib C$^{\beta}$H), 2.83 (m, 2H, Tyr C$^{\beta}$H), 3.5 (s, 3H, Tyr OMe), 4.42 (m, 1H, Tyr C$^{\alpha}$H), 6.52 (m, 2H, aromatic proton), 6.89−6.94 (m, 4H, aromatic proton), 7.12 (m, 2H, aromatic proton), 7.25−7.29 (m, 4H, aromatic proton and Tyr-NH), 7.73 (m, 2H, aromatic proton), 8.29 (s, 1H, Aib-NH), 9.16 (b, 1H, phenolic OH),9.33 (d, 1H, NPA-NH). ^{13}C NMR (100 MHz, DMSO-d_6, δ ppm): 24.72, 24.82, 39.09, 51.65, 53.76, 56.36, 114.9, 115.26, 118.22, 119.23, 119.77, 121.58, 127.09, 129.32, 129.67, 130.07, 131.86, 141.79, 143.92, 155.76, 168.22, 172, 173.85. Mass spectral data TOF-MS m/z: $[M + Na]^+$, 498.2374.

*Fenamic Acid−Aib-Maba-OMe (Peptide **3**).* A 500 mg (1.68 mmol) of NPA-Aib-OH wasdissolved in 25 mL of dry DCM in an ice−water bath. A 0.7 g (3.35 mmol) of DCC was added in the reaction mixture. H-MABA-OMe was extracted from 0.63 g (3.35 mmol) of the corresponding methyl ester hydrochloride by neutralization and subsequent extraction with ethyl acetate, and ethyl acetate was evaporated; then, it was dissolved to dry DCM and added to the reaction mixture immediately after the addition of DCC. The reaction mixture was allowed to come to room temperature and stirred for 48 h. Then, DCM was evaporated, the residue was dissolved in ethyl acetate (60 mL), and DCU was filtered off. A 2 M HCl (3 × 50 mL), 1 M sodium carbonate (3 × 50 mL), and brine (2 × 50 mL) were used to wash the organic layer, and the organic layer was dried over anhydrous sodium sulfate and evaporated in a vacuum to obtain peptide **3** as a solid. Silica gel (100−200 mesh) and hexane−ethyl acetate (4:1) as an eluent were used for the purification of the compound. Yield: 0.43 g (1 mmol, 60%). ^{1}H NMR (400 MHz, $CDCl_3$, δ ppm): 1.65 (s, 6H, Aib C$^{\beta}$H), 3.79 (s, 3H, Maba-OMe protons), 6.74−6.78 (m, 2H, aromatic proton), 6.92 (m, 1H, aromatic proton), 7.09−7.18 (m, 2H, aromatic proton), 7.18−7.3 (m, 5H, aromatic proton), 7.45 (m, 1H, aromatic proton), 7.68 (m, 1H, aromatic proton), 7.74 (m, 1H, aromatic proton), 8.01 (s, 1H, Aib-NH), 8.89 (s, 1H, Maba NH), 9.02 (s, 1H, NPA NH). ^{13}C NMR (100 MHz, $CDCl_3$, δ ppm): 25.63, 25.77, 52.38, 58.93, 116.57, 118.77, 121.02, 121.24, 122.99, 124.79, 125.49, 128.31, 129.25, 129.57, 133.09, 138.46, 141.29, 145.69, 166.95, 170.18, 172.69. Mass spectral data TOF-MS m/z: $[M + Na]^+$, 454.1425.

NMR Experiments. All the compounds (1−10 mM) in DMSO-d_6 and $CDCl_3$ solution are characterized by NMR spectroscopy on a JEOL (400 MHz) spectrometer or a Bruker (500 MHz) spectrometer. Tetramethylsilane (d = 0.0 ppm) was used as an internal standard.

FT-IR Experiments. All the compounds are characterized by FT-IR spectroscopy in solid state by forming KBr palette in a PerkinElmer Spectrum RX1 spectrophotometer.

Absorption Spectroscopy. A UV/vis spectrometer (MAPADA UV-6300) and a 1 cm path-length quartz cell were used to record the absorption spectra of the compounds.

Fluorescence Spectroscopy. The fluorescence spectra were recorded on a JASCO spectrofluorometer (FP-8300) using a quartz cell having a 1 cm path length; 5/5 slit widths were used.

Mass Spectrometry. All the compounds were characterized by mass spectrometry on a Waters Corporation Q-Tof Micro YA263 high-resolution mass spectrometer by electrospray ionization (positive mode).

POM. The morphology of the compounds was determined by POM images. A small amount of the solution of the compound was drop-casted on a clean glass slide, dried by slow evaporation, and then visualized at 40× magnification on an Olympus optical microscope equipped with a polarizer and a charge-coupled device (CCD) camera.

Field Emission Scanning Electron Microscopy. The morphologies of the synthesized peptides were examined by FE-SEM. The peptide solution was drop-casted on a clean glass coverslip and dried under a vacuum. The images were captured in an FE-SEM apparatus (Jeol Scanning Microscope-JSM-6700F) by gold coating.

Gelation. The peptide **3** (25 mg) was mixed in 1 mL of xylene and 1 mL of water, and gel was obtained by the heating−cooling technique.

Transmission Electron Microscopy. TEM was performed to examine the morphology of the synthesized gel of peptide **3**. A slice of the phase-selective gel was placed on a clean copper grid and dried under a vacuum. The images were captured in a TEM apparatus (JEM2100Plus).

X-ray Crystallography. Diffraction-quality crystals of peptides **1**−**3** were obtained from solution by slow evaporation. Intensity data were collected with Mo Kα (peptide **1** and **2**) or Cu Kα (peptide **3**) radiation by a Bruker APEX-2 CCD diffractometer. The data were processed using Bruker SAINT package. The structure solution and refinement were performed by SHELX97. Refinement of nonhydrogen atoms was performed using anisotropic thermal parameters. CCDC 197545, 1960546, and 1960544 contain the crystallographic data for the peptides **1**−**3**, respectively.

■ ASSOCIATED CONTENT

Supporting Information

The Supporting Information is available free of charge at https://pubs.acs.org/doi/10.1021/acsomega.9b03532.

Crystallographic information for NPAP (CIF)

Synthesis and characterizations of peptides; ^{1}H NMR, ^{13}C NMR, and MS results of Fenamic acid−Aib-Maba OMe **3**; concentration-dependent UV-Vis spectra and fluorescence spectra of peptides; and POM images of peptides (PDF)

https://dx.doi.org/10.1021/acsomega.9b03532
ACS Omega 2020, 5, 2287−2294

Crystallographic information for NPAM (CIF)
Crystallographic information for NPAT (CIF)

AUTHOR INFORMATION

Corresponding Author

Debasish Haldar − *Department of Chemical Sciences, Indian Institute of Science Education and Research Kolkata, Mohanpur 741246, India;* orcid.org/0000-0002-7983-4272; Email: deba_h76@yahoo.com, deba_h76@iiserkol.ac.in

Authors

Srayoshi Roy Chowdhury − *Department of Chemical Sciences, Indian Institute of Science Education and Research Kolkata, Mohanpur 741246, India*

Sujay Kumar Nandi − *Department of Chemical Sciences, Indian Institute of Science Education and Research Kolkata, Mohanpur 741246, India*

Debasish Podder − *Department of Chemical Sciences, Indian Institute of Science Education and Research Kolkata, Mohanpur 741246, India*

Complete contact information is available at: https://pubs.acs.org/10.1021/acsomega.9b03532

Author Contributions

S.R.C. has synthesized the compounds. S.R.C., S.K.N., and D.P. have performed the experimental works. D.H. has done the analysis and wrote the manuscript.

Notes

The authors declare no competing financial interest.

ACKNOWLEDGMENTS

This work is supported by CSIR, India (fellowship to S.R.C., S.K.N., and D.P.).

REFERENCES

(1) Cruz-Cabeza, A. J.; Bernstein, J. Conformational Polymorphism. *Chem. Rev.* **2014**, *114*, 2170−2191.

(2) Appavoo, S. D.; Huh, S.; Diaz, D. B.; Yudin, A. K. Conformational Control of Macrocycles by Remote Structural Modification. *Chem. Rev.* **2019**, *119*, 9724−9752.

(3) Hecht, S.; Huc, I. *Foldamers: Structure, Properties, and Applications*; Wiley-VCH: Weinheim, 2007.

(4) Gellman, S. H. Foldamers: A Manifesto. *Acc. Chem. Res.* **1998**, *31*, 173−180.

(5) Hill, D. J.; Mio, M. J.; Prince, R. B.; Hughes, T. S.; Moore, J. S. A Field Guide to Foldamers. *Chem. Rev.* **2001**, *101*, 3893−4012.

(6) Karle, I. L.; Pramanik, A.; Banerjee, A.; Bhattacharjya, S.; Balaram, P. ω-Amino Acids in Peptide Design. Crystal Structures and Solution Conformations of Peptide Helices Containing a β-Alanyl-γ-Aminobutyryl Segment. *J. Am. Chem. Soc.* **1997**, *119*, 9087−9095.

(7) Roy, R. S.; Gopi, H. N.; Raghothama, S.; Karle, I. L.; Balaram, P. Hybrid Peptide Hairpins Containing α- and ω-Amino Acids: Conformational Analysis of Decapeptides with Unsubstituted β-, γ-, and δ-Residues at Positions 3 and 8. *Chem.—Eur. J.* **2006**, *12*, 3295−3302.

(8) Rai, R.; Vasudev, P. G.; Ananda, K.; Raghothama, S.; Shamala, N.; Karle, I. L.; Balaram, P. Hybrid Peptides: Expanding the β Turn in Peptide Hairpins by the Insertion of β-, γ-, and δ-Residues. *Chem.—Eur. J.* **2007**, *13*, 5917−5926.

(9) Yin, H.; Hamilton, A. D. Strategies for targeting protein-protein ineractions with synthetic agents. *Angew. Chem., Int. Ed.* **2005**, *44*, 4130−4163.

(10) Kim, Y.-W.; Grossmann, T. N.; Verdine, G. L. Synthesis of allhydrocarbon stapled α-helical peptides by ring-closing olefin metathesis. *Nat. Protoc.* **2011**, *6*, 761−771.

(11) Muppidi, A.; Doi, K.; Edwardraja, S.; Drake, E. J.; Gulick, A. M.; Wang, H.-G.; Lin, Q. Rational design of proteolytically stable, cellpermeable peptide-based selective Mcl-1 inhibitors. *J. Am. Chem. Soc.* **2012**, *134*, 14734−14737.

(12) Taylor, J. W. The synthesis and study of side-chain lactam-bridged peptides. *Biopolymers* **2002**, *66*, 49−75.

(13) Kumar, M. G.; Thombare, V. J.; Katariya, M. M.; Veeresh, K.; Raja, K. M. P.; Gopi, H. N. Non-classical helices with cis carbon-carbon double bonds in the backbone: structural features of α,γ-hybrid peptide foldamers. *Angew. Chem., Int. Ed.* **2016**, *55*, 7847−7851.

(14) Debnath, M.; Das, T.; Podder, D.; Haldar, D. α,ε-Hybrid Peptide Foldamers: Self-assembly of Peptide with trans Carbon-Carbon Double Bonds in the Backbone and its Saturated Analogue. *ACS Omega* **2018**, *3*, 8760−8768.

(15) Maity, S. K.; Maity, S.; Jana, P.; Haldar, D. Supramolecular double helix from capped γ-peptide. *Chem. Commun.* **2012**, *48*, 711−713.

(16) Jana, P.; Maity, S.; Maity, S. K.; Haldar, D. A new peptide motif in the formation of supramolecular double helices. *Chem. Commun.* **2011**, *47*, 2092−2094.

(17) Haldar, D.; Schmuck, C. Metal free double helices from abiotic backbone. *Chem. Soc. Rev.* **2009**, *38*, 363−371.

(18) Maity, S.; Jana, P.; Maity, S. K.; Kumar, P.; Haldar, D. Confo mational heterogeneity, self-assembly and gas adsorption studies of isomeric hybrid peptides. *Cryst. Growth Des.* **2012**, *12*, 422−428.

(19) Mondal, S.; Bairi, P.; Das, S.; Nandi, A. K. Phase selective organogel from an imine based gelator for use in oil spill recovery. *J. Mater. Chem. A* **2019**, *7*, 381−392.

(20) Okesola, B. O.; Smith, D. K. Applying low-molecular weight supramolecular gelators in an environmental setting − selfassembled gels as smart materials for pollutant removal. *Chem. Soc. Rev.* **2016**, *45*, 4226−4251.

(21) Bhattacharya, S.; Krishnan-Ghosh, Y. First report of phase selective gelation of oil from oil/water mixtures. Possible implications toward containing oil spills. *Chem. Commun.* **2001**, 185−186.

(22) Kar, T.; Debnath, S.; Das, D.; Shome, A.; Das, P. Organogelation and Hydrogelation of Low-Molecular-Weight Amphiphilic Dipeptides: pH Responsiveness in Phase-Selective Gelation and Dye Removal. *Langmuir* **2009**, *25*, 8639−8648.

(23) Prathap, A.; Sureshan, K. M. Organogelator−Cellulose Composite for Practicaland Eco-Friendly MarineOil-Spill Recovery. *Angew. Chem., Int. Ed.* **2017**, *56*, 9405−9409.

(24) Wang, D.; Niu, J.; Wang, Z.; Jin, J. Monoglyceride-Based Organogelator for Broad-Range Oil Uptake with High Capacity. *Langmuir* **2015**, *31*, 1670−1674.

(25) Ren, C.; Ng, G. H. B.; Wu, H.; Chan, K.-H.; Shen, J.; Teh, C.; Ying, J. Y.; Zeng, H. Instant Room-Temperature Gelation of Crude Oil by Chiral Organogelators. *Chem. Mater.* **2016**, *28*, 4001−4008.

(26) Cui, Y.; Li, M.-C.; Wu, Q.; Pojman, J. A.; Kuroda, D. G. Synthesis Free Phase-Selective Gelator for Oil-Spill Remediation. *ACS Appl. Mater. Interfaces* **2017**, *9*, 33549−33553.

(27) Maity, S.; Jana, P.; Haldar, D. Fabrication of nanoporous material from a hydrophobic peptide. *CrystEngComm* **2011**, *13*, 3064−3071.

(28) Hamiaux, C.; Drummond, R. S. M.; Luo, Z.; Lee, H. W.; Sharma, P.; Janssen, B. J.; Perry, N. B.; Denny, W. A.; Snowden, K. C. Inhibition of strigolactone receptors by N-phenylanthranilic, acid derivatives: Structural and functional insights. *J. Biol. Chem.* **2018**, *293*, 6530−6543.

(29) Das, K. R.; Antony, M. J.; Varghese, S. Highly bluish-white light emissive and redox active conjugated poly-Nphenyl anthranilic acid polymer fluoroprobe for analytical sensing. *Polymer* **2019**, *181*, 121747−121757.

(30) Moretto, V.; Crisma, M.; Bonora, G. M.; Toniolo, C.; Balaram, H.; Balaram, P. Comparison of the effect of five guest residues on the .beta.-sheet conformation of host (L-val)n oligopeptides. *Macromolecules* **1989**, *22*, 2939−2944.

(31) Okesola, B. O.; Smith, D. K. Applying low-molecular weight supramolecular gelators in an environmental setting−selfassembled gels as smart materials for pollutant removal. *Chem. Soc. Rev.* **2016**, *45*, 4226−4251.
(32) Podder, D.; Chowdhury, S. R.; Nandi, S. K.; Haldar, D. Tripeptide based super-organogelators: structure and function. *New J. Chem.* **2019**, *43*, 3743−3749.
(33) Prathap, A.; Sureshan, K. M. Organogelator-cellulose composite for practical and eco-friendly marine oil spill recovery. *Angew. Chem., Int. Ed.* **2017**, *56*, 9405−9409.

https://dx.doi.org/10.1021/acsomega.9b03532
ACS Omega 2020, 5, 2287−2294